ORIGINAL ARTICLE

Production of efficient carbon fiber from different solid waste residuals for adsorption of hazardous metals from wastewater samples

Ayman F. Abou-Hadid[1] · Usama A. El-Behairy[1] · Mahmoud M. Elmalih[2] · Enas Amdeha[3] · Ahmed M. A. El Naggar[3] · Mohamed H. Taha[2] · Ahmed E. M. Hussein[2]

Abstract

Uranium (as a hazardous and radioactive element) removal from wastewater requires reliable technology and proper functional materials. Carbon fiber species that are produced from agricultural solid waste can be a proper type of low-cost adsorbents for wide uses in wastewater treatment. In this work, two carbon fiber species labeled CF-RH and CF-SCB were synthesized from two different agricultural wastes, namely, rice husk and sugarcane bagasse respectively. The structural properties of carbon fiber were verified by XRD, FTIR, and Raman, spectroscopy. Both nitrogen-adsorption–desorption BET surface area and TEM were performed to figure out the textural characteristics of the presented sorbents. The charges on surfaces of the fibers were detected via zeta potential analysis. The prepared carbon fibers were applied for uranium removal from aqueous solution by adsorption technique. The acquired data display that the equilibrium time was 240 min. The results of adsorption process are nicely fitted with pseudo-second-order-kinetic and Langmuir isotherm models. The maximum sorption capacity was 21.0 and 29.0 mg/g for CF-RH and CF-SCB, respectively. Sorption thermodynamics declare that adsorption of U(VI) is an endothermic, spontaneous, and feasible process. The picked findings of this study could emphasize high reliability of the introduced adsorbents in efficient tackling of water contaminants.

Keywords Adsorption process · Agricultural solid residuals · Carbon fiber species · Metal recovery · Wastewater decontamination

1 Introduction

The green revolution increases the agricultural land which in turn enhances the agricultural production by triple and increases the yields to meet the demands of a rapidly growing global population [1]. Globally, the agricultural wastes negatively influence the water resources, air, and the soil, which thus risking the sustainability of ecological environment and the human health [2, 3]. Uranium mining as well as nuclear activities produces liquid effluents contaminated with radioactive elements [4, 5]. The release of these effluents without treatment is also jeopardizing not only the ecosystems but also the human bodies [5, 6]. Therefore, the application of agricultural waste for wastewater treatment is considered as an interesting approach for environmental security and protecting human lives.

Various conventional approaches were applied for reclamation of radioactive industrial liquid effluents, for instance, bioprecipitation [7], reductive precipitation [8], ion change [9, 10], and adsorption [11–13]. Among all these mentioned techniques, adsorption is a talented method for uranium species illumination from wastewater owing to its simplicity, effectiveness, and feasibility [13, 14]. Activated carbon derived from agricultural wastes (a biomass byproduct from the agricultural system) is a cost-effective sorbent for wastewater treatment [15–17].

✉ Enas Amdeha
enas_amdeha@yahoo.com

✉ Ahmed M. A. El Naggar
drmeto1979@yahoo.com

1   Faculty of Agriculture, Ain Shams University, Cairo, Egypt

2   Nuclear Materials Authority, El Maddi, P.O. Box 530, Cairo, Egypt

3   Egyptian Petroleum Research Institute (EPRI), 1 Ahmed El-Zomor St., Nasr City, Cairo, Egypt

Biomass waste valorization is one of the most current concerns being researched around the world to develop sustainable solutions that work hand in hand with the expansion of the circular economy model [18, 19]. The most plentiful renewable raw material for achieving these aims is lignocellulosic biomass, which is made up of glucose and lignin [20]. Rice husk (RH) and sugarcane bagasse (SCB) are two of the most interesting biomasses composed mainly of cellulose, hemicelluloses, and lignin.

Rice husk (RH), an agricultural waste produced in large quantities from rice milling around the world, is regarded as a waste product that is burned in the open air or buried in a wasteland, causing severe environmental disposal issues [21]. RH has a complex composition of hydrocarbons and silicates, but it appears to be an appropriate material for the synthesis of activated carbons once the volatile constituents are removed by carbonization [22].

Sugarcane bagasse (SCB) is the prime byproduct of the sugarcane industry, accounting for roughly 30% of total sugarcane production weight. Sugarcane production in the world is around 1900 million tons per year and is anticipated to be rising to around 0.6 billion tons by 2024 [20, 23]. The use of RH and SCB as adsorbents to sequester hazardous environmental pollutants is widely documented in the literature [23, 24].

However, nowadays, agro-industrial residue-based adsorbents are mostly employed in modified states, which increase their adsorption capabilities, most likely due to reinforced porosity, increased functional groups, or increased surface area. Activation, carbonization, grafting, chemical treatment, and composite production are the most prevalent modification processes [24]. Because of their economic feasibility, ease of synthesis, hetero-porous architectures, and high adsorption performance, carbon fibers synthesized from natural, low-cost, and abundant biomass are considered environmentally acceptable adsorbent materials [25].

In this study, RH and SCB as biomass wastes are used to prepare carbon fiber by a facile method. The structures of the obtained carbon fibers were characterized by XRD, FTIR, Raman, N2 adsorption–desorption isotherms, zeta, and TEM. The adsorption behavior of the prepared biomass wastes-based carbon fiber is studied toward the removal and recovery of and uranium ions from aqueous solutions. Adsorption isotherm, kinetics, and thermodynamics were investigated.

2 Experimental

2.1 Materials

Hydrochloric acid (HCl, $\geq 36\%$), sulfuric acid (H$_2$SO$_4$, $\geq 98\%$), and nitric acid (HNO$_3$, $\geq 63\%$) were

reagent grade and supplied from Adwic, Egypt. Stock solution of uranium (1000 mg L^{-1}) was prepared using UO$_2$(NO$_3$)$_2$.6H$_2$O (Aldrich, USA). Fresh prepared uranium standard solutions with specific initial concentrations were attained by diluting the U(VI) stock solution using deionized water. Hydrochloric (0.5 mol L^{-1}) and/or sodium hydroxide (0.5 mol L^{-1}) solutions were utilized to adjust the pH of uranium solutions. Rice husk (RH) was collected from a farm in Al-Gharbiya Governate, Egypt. Sugarcane bagasse (SCB) was collected from a sugarcane juice shop in Cairo, Egypt.

2.2 Preparation of carbon fiber

Waste-generated carbon fibers (CF) are used as green adsorbents to remove uranium species from aqueous solution. Rice husk (RH) and sugarcane bagasse (SCB) are used as agricultural wastes to produce natural carbon fiber as a valuable resource for adsorption purposes. For 1 week, the raw waste was dried in a 90 °C oven. After drying the sample, it was calcined in a muffle furnace for 6 h at 500 °C. A heating rate of 25 °C/min was used in the calcination process. The natural fiber's black color was attained after the sample was cooled to room temperature [26]. The carbon fiber from RH and SCB is abbreviated as CF-RH and CF-SCB, respectively.

2.3 Characterization of carbon fiber

An X-ray diffractometer (XRD, Shimadzu XD-1, Japan) was employed to determine the XRD patterns. Fourier transform infrared spectrophotometer (FTIR, Nicolet Is-10 model, USA) was applied to get FTIR by adopting the KBr technique. Raman spectrometer (BRUKER-SENTERRA, Germany) equipped with an integral microscope (Olympos) was applied to identify the carbon fiber. An N$_2$ adsorption–desorption isotherm (a NOVA 3200 apparatus, USA) at -196 °C was applied to analyze the surface properties. A dynamic light scattering (DLS, Malvern-ZS, Ltd., UK, nanoseries) was employed for the zeta potential measurements. A high-resolution transmission electron microscope (TEM, JEM 1230, JEOL, Japan) was employed to execute the morphology of the samples. Inductively coupled plasma optical emission spectrometer model Optima 2100DV (Perkin-Elmer, USA) was used for U(VI) measurement as well as chemical analysis for the waste working sample. Solution pH was detecting using Orion pH/mv 910 ion analyzer with accuracy $= \pm 0.01$. Batch experiments were conducted using G.F.L 1083, thermostatic shaking water bath, Germany (working temperature range of 25–100 °C).

2.4 U(VI) sorption experiments

Uranium sorption onto CF-RH and CF-SCB sorbents was evaluated by performing a set of experiments using batch method. In polyethylene tube, a certain weight of the solid material (m, g) was added to a specific volume (V, L) of fresh prepared uranium standard solution with certain initial concentration (Co, mg L^{-1}) for period of time interval of 5–600 min using thermostatic shaking water bath. The sorption experiments were carried out in duplicate, and the mean value of ≤4% relative error was accepted. Solid/ liquid separation was achieved using 0.2-μm syringe filters. U(VI) residual concentration (Ce, mg L^{-1}) was measured using ICP-AES. The following equations were applied to calculate the sorption capacity qe (mg g^{-1}), sorption efficiency %, and the dimensionless distribution constant (K_C) [10].

$$q_e = \left(C_o - C_e\right)X\frac{V}{m}\text{x} \tag{1}$$

$$R\% = \frac{\left(C_o - C_e\right)}{C_o}X100 \tag{2}$$

$$K_C = \left(\frac{q_e}{C_e}X1000\right) \tag{3}$$

3 Results and discussion

3.1 Sorbent characterizations

3.1.1 XRD analysis

Figure 1 represents the XRD spectra of the prepared CF-RH and CF-SCB to study their structure. As carbon fibers from RH and SCB are lignin-based carbon fibers, a broad peak in the range 15°–39° exists in the spectra of both samples as a result of the amorphous carbon structure. Moreover, this band reveals the stacking of the graphitic plates [27]. The peak near 2θ = 28.3° is for the (0 0 2) plane of the graphite and can be related to the carbon fiber graphitic region. The interlayer spacing d_{002} value is 0.315 nm for both CF-RH and CF-SCB. The (1 0 0) planes' peaks have appeared at 40.5° and 45° and 40.6° and 50.2° for CF-RH and CF-SCB samples, respectively. These peaks are for the graphitic structure and have also been observed in previous carbon fibers experiments. These peaks correspond to the graphitic structure and have previously been seen by Liu et al. (2008) [28] and Poursorkhabi et al. (2020) [29].

3.1.2 FTIR analysis

Figure 2 shows how FTIR is used to check that all the chemical groups other than carbon have been removed completely from carbon fiber samples. For the CF-SCB sample, there is broadband with a reasonable intensity at 3620–3860 cm^{-1}, whereas the band is shifted for the CF-RH sample to be around 3470 cm^{-1}. This band is caused by the moisture-induced O–H vibrational bending and stretching of both OH groups and adsorbed H$_2$O. Additionally, the presence of H-bonds between the OH groups is responsible for this band [30]. The band at 1100–1110 cm^{-1} in the spectra of CF samples is the carbon fingerprint and is related to the C–O symmetric and asymmetric stretching vibration of –C–O–C– ring [31]. The peaks at 792 cm^{-1}, 620 cm^{-1}, and 454 cm^{-1} could be caused by the C–H vibrations. There are additional peaks that appeared in the CF-SCB sample and not in the CF-RH sample due to the different compositions of the raw materials. The CF-SCB sample exhibits two
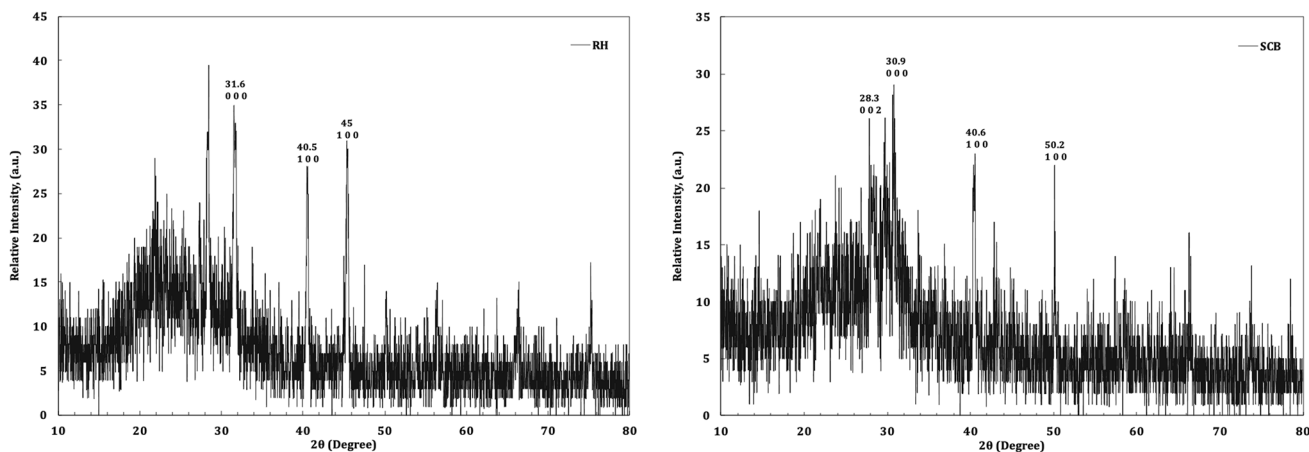
Fig. 1 XRD spectra of carbon fiber produced from RH and SCB
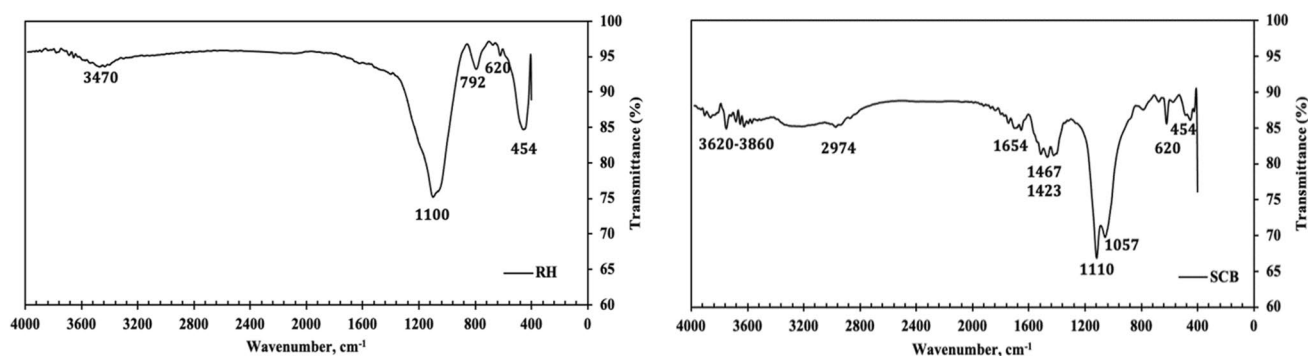
Fig. 2 FTIR spectra of carbon fiber produced from RH and SCB

peaks around 2974 cm^{-1} and 1654 cm^{-1} for the C–H aliphatic axial deformation in CH$_2$ and CH$_3$ groups and C–O stretching vibration, respectively. These peaks appear for samples-based cellulose, lignin, and hemicelluloses [27]. The peaks at 1467 cm^{-1} and 1423 cm^{-1} could be related to the C–H bending vibration of CH$_2$ and the –COOH groups, respectively [32]. Besides, the peak at 1057 cm^{-1} is for C–O groups and unconjugated C = O stretch that exist in the lignin-based carbonized fibers [27].

3.1.3 Raman analysis

The carbonization process converts the biomass (RH and SCB) to the graphite structure, and the graphitization degree changes according to the material's nature and temperature. The CF samples are composed totally of C–C bonds with different bonds orientation according to the sample structure. Raman spectroscopy as a valuable, powerful, and highly sensitive technique to even slight changes in C–C bonds orientation is suitable to provide a wealth of information about the carbon fiber structure (Fig. 3). Raman spectroscopy has long been used to investigate the vibrational properties of sp^2-hybridized carbons and provide valuable insight into the sp^2–sp^3

hybridization ratio [33]. Carbon materials have two feature bands which are called the D band and G band. The D band, the disorder band or the defect band, is present in all graphite-like carbons and originates from a hybridized vibrational mode associated with carbon edges, and it indicates the presence of structural defects [34]. Moreover, this band is called "turbostratic carbon structure" [29]. The G band (1595 cm^{-1}) explains the degree of graphitization [34], and it exists due to the carbon hybridization (sp^2) as well as the stretching mode in the C–C bond in the graphitic materials [29].

The CF-RH sample spectrum exhibits the typical features of carbon materials with two bands at 1340 cm^{-1} (D band) and 1595 cm^{-1} (G band), and these bands are related to out of plane and in-plane sp^2 carbon bonds, respectively [35], while the CF-SCB samples exhibit only a vibrational mode (D band) at 1302 cm^{-1} related to disordered carbons [17]. The presence of such D-band suggests the amorphous nature of CF-SCB. A breakdown of the k-selection rule causes the Raman intensity of the D band to be inversely proportional to crystallite size. The I_D/I_G ratio is frequently used to measure the degree of fiber structural disorder. This is the ratio of the disorder-induced band's integrated intensity to the Raman-allowed
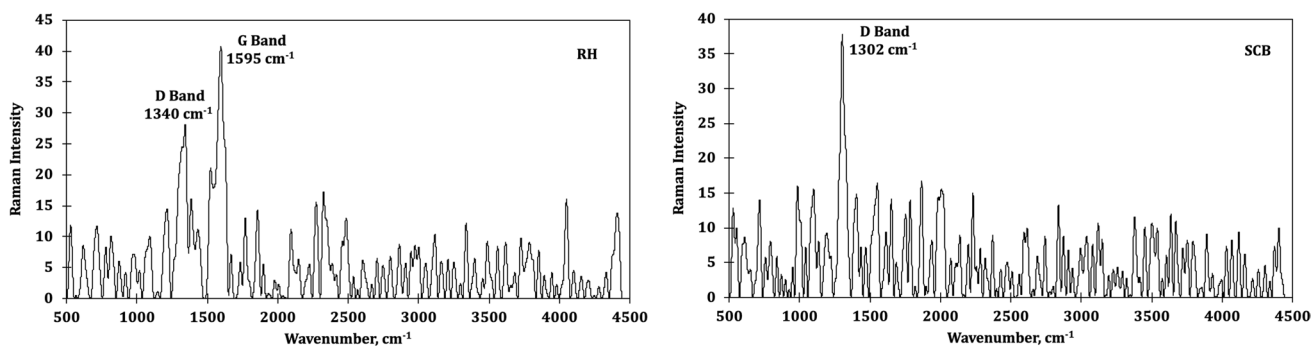
Fig. 3 Raman spectra of carbon fiber produced from RH and SCB

band's integrated intensity [35]. Furthermore, as this ratio provides a gauge for the number of structural defects and quantifies the measure of edge plane exposure, this ratio is commonly used as an indicator of structural order [34]. A fiber with high defects exhibits a high ratio of I_D/I_G [32]. The I_D/I_G of the CF-RH is equal to 0.68. Impurities are responsible for other minor peaks [36].

3.1.4 BET

The N2 adsorption/desorption isotherms and the pore size distributions for CF-RH and CF-SCB are displayed in Fig. 4. The isotherm curves show a hysteresis loop at a relative pressure of 0.1–0.9 indicating the type IV and H3 hysteresis loop based on the IUPAC classification [37]. The hysteresis curves represent the mixture of micro- and mesopore structures dominated by mesopores [38]. The existence of these pores in the lignin fibers during the carbonization process by the removal of volatile material enhances its structural properties [29]. Type IV isotherm is also shown by various biomass like cassava peel [39] and banana stem fibers [40]. It has been proposed that the shape of the hysteresis loop and the texture (pore size and pore geometry) of porous materials are related. The pores were discovered to have a slit-shaped structure [27]. The surface area of CF-RH is 14.49 m^2/g, which is higher than CF-SCB (8.75 m^2/g). This result indicates that the raw material composition has a crucial role on the surface area of the obtained carbon fibers. Additionally, the total pore volume and the average pore diameter are 0.046 cm^3/g, 12.83 nm, and 0.029 cm^3/g, 13.32 nm for CF-RH and CF-SCB, respectively.

3.1.5 Zeta potential

The electrical potential of the CF surface layer has a great role in the adsorption process. This potential is measured as zeta potential. As the adsorbent zeta potential increased in

	pH 3	pH 5	pH 7	pH 9
RH	0.0303	-30.6	-26.9	-24.1
SCB	-0.676	-31.9	-29	-0.0831
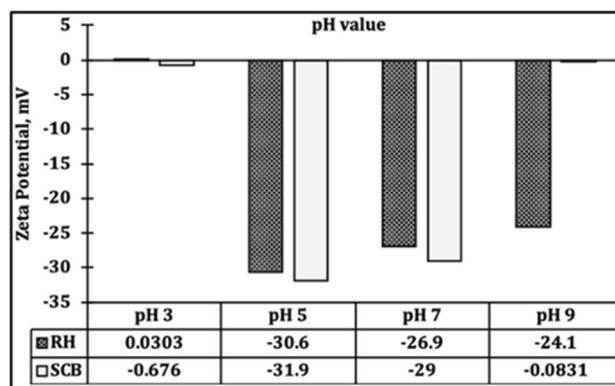
Fig. 5 Zeta potential of the carbon fiber from RH and SCB as a function of pH

the opposite charge of the adsorbate, the adsorption process enhanced. For the CF-RH sample, the negative zeta potential increases with decreasing the pH from pH 9 to pH 5 at which the zeta potential attains its maximum value (−30.6 mV), while, for the CF-SCB sample, the negative zeta potential is −29 mV and −31.9 mV at pH 7 and pH 5, respectively, which is higher than that of the CF-RH sample (Fig. 5). As the zeta potential for both CF samples at pH 5 is higher than 30 mV, it reveals that the particles are distributed in a good manner, and the solution with CF particles is a stable suspension that may enhance the adsorption behavior of these samples [38]. As the change in the solution pH influences the metal adsorption process, the preferred pH range for the adsorption of the positively charged metal on the negatively charged CF is 5–7 pH.

3.1.6 TEM

The CF surface morphology is observed with TEM, and the images are shown in Fig. 6. The nature and composition of the used biowaste affect the CF microstructural properties.
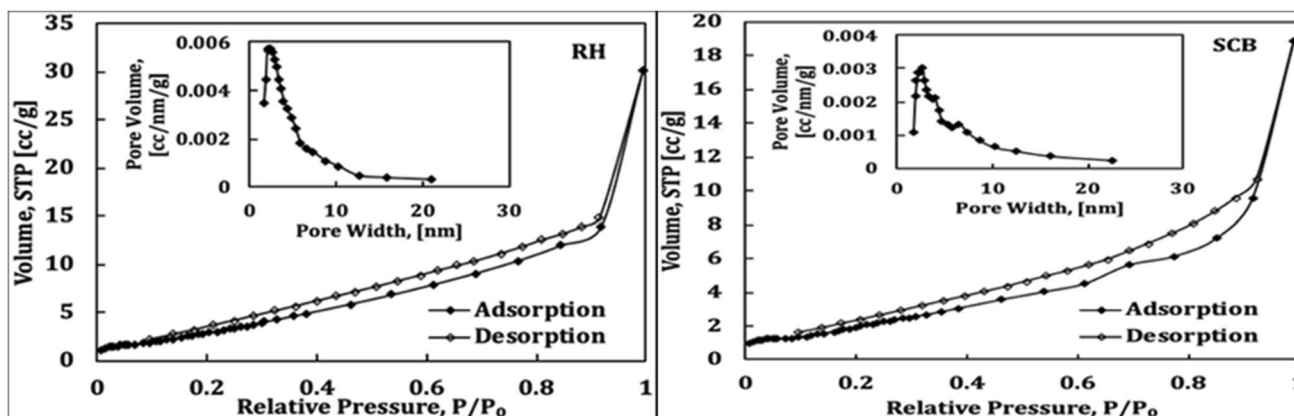
Fig. 4 N$_2$ adsorption–desorption isotherm at −196 °C for carbon fiber produced from RH and SCB. Inset: the pore size distribution curve

Both CF-RH and CF-SCB are biowaste-based CF, and these biowastes mainly compose of cellulose, hemicellulose, lignin, and ash. The intrinsic hierarchical structure makes these biowastes appropriate carbon precursors that produce porous carbon with boosted adsorption behavior [41]. From the CF images, a reasonably amorphous nature could be observed, though there are clusters formed from the agglomerated particles. Figure 6 displays that the CF particles have a dual nature of both amorphous and crystalline appearance. There are small crystals possessing different shapes embedded within the large char particles. The porous structure of CF-RH and CF-SCB has approximately 12 to 14 nm pore dimensions which are coincident with the BET measurements. It again indicates that the CF structure consists of both crystalline and amorphous structures, exhibiting the turbostratic nature.

3.2 Sorption investigation

3.2.1 Effect of solution pH

Solution pH plays an important role in the adsorption of uranium species from aqueous solution, whereas it controls the surface functional group charge and binding sites of the adsorbent. Figure 7 explores the influence of solution pH on the uranium sorption percent using CF-RH and CF-SCB carbonaceous materials. The solution pH in the range of 1–8 was performed by applying the following parameters: stirring time (240 min), U(VI) concentration (50 mg L^{-1}), and room temperature. The explored results declare that both CF-RH and CF-SCB sorbents exhibit the same sorption behavior, whereas the sorption plot consists of two regions. The first regen extends from pH 1 to 4 and is characterized by gradual increase in the sorption percent as the solution pH increases. This performance is owned to the presence of H+ ions at high concentration which make high competition with uranium cationic species ($UO_2NO_3^+$ and UO_2^{2+}) for binding to the sorbent active surface [12, 13]. The increase of solution pH shows a decrease in the H+ ions concentration which give more chance for the interaction of U(VI) cationic species with sorbent active function groups [42, 43]. The second stage appears at pH > 4 and is depicted with dramatically ramp down of the sorption percent which could attributed to the disappear of U(VI) cationic species and the presence of uranium insoluble species [42, 43]. The same sorption performance has been reported for U(VI) sorption

Fig. 6 TEM of carbon fiber produced from RH (**a**, **b**) and SCB (**c**, **d**)
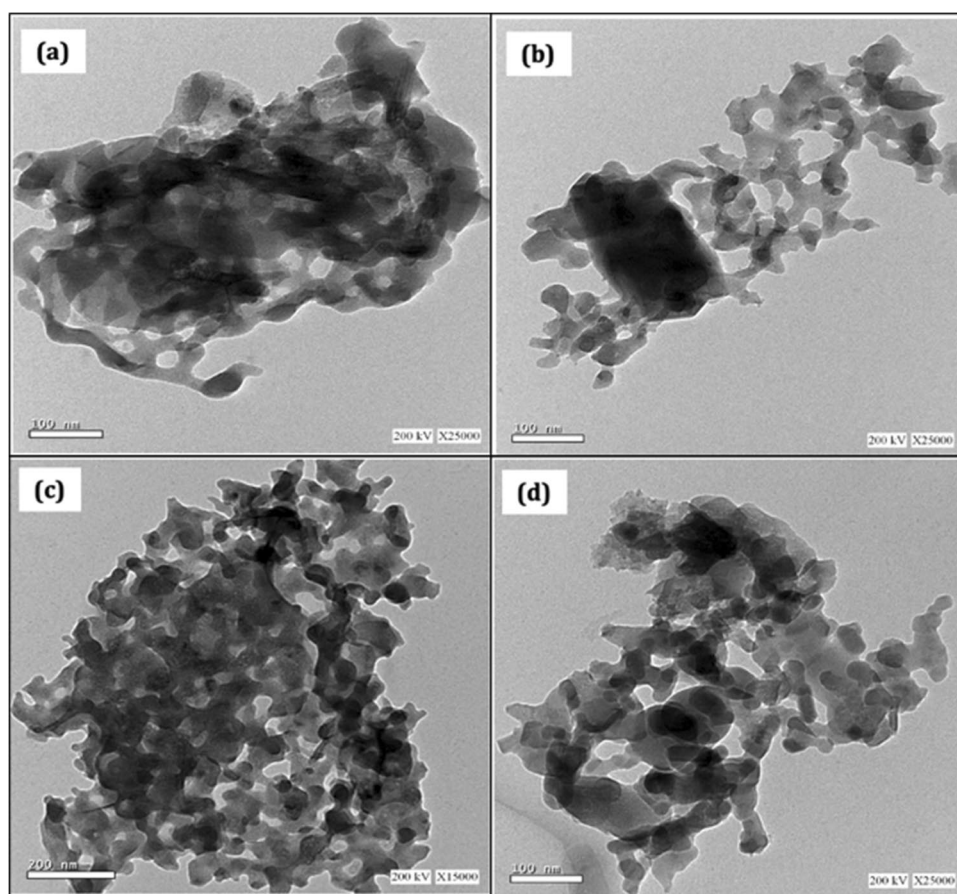
Fig. 7 U(VI) sorption efficiency, % (2.0 g sorbent/ L; initial concentration 50 mg L.$^{-1}$; temperature 298 K)
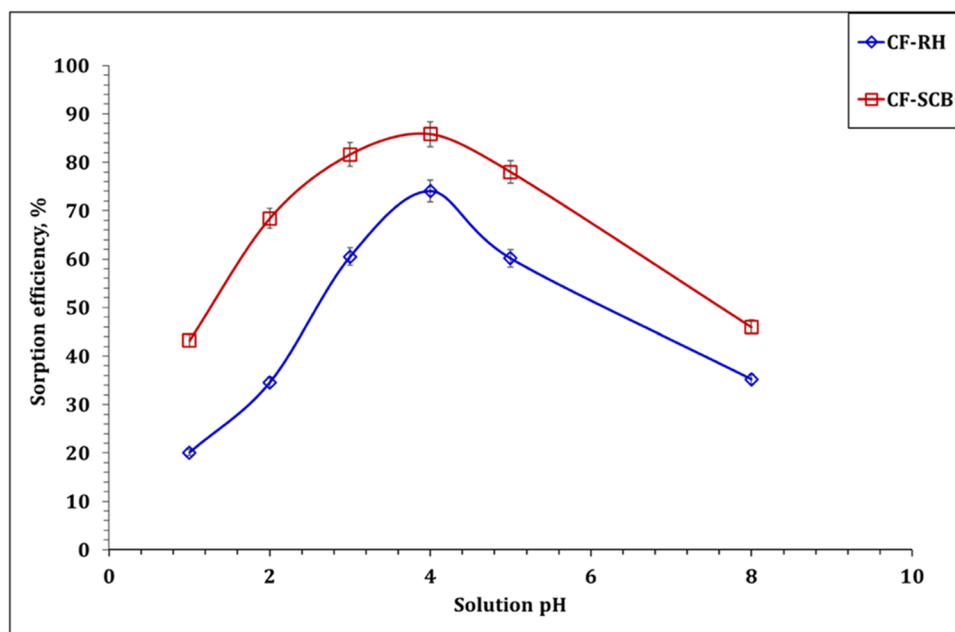
3.2.2 Effect of contact time and reaction kinetics

The dependence of U(VI) sorption efficiency as a function of contact time has been investigated by conducting a set of experiments at reaction time interval 5–600 min, while other parameters were fixed at solution pH of 4.01, sorbent dose of 2 g L^{-1}, reaction temperature of 298 ± 1 K, and U(VI) initial concentration of 50 mg L^{-1}. The variation of sorption percent with time is presented in Fig. 8. The acquired results obvious that the sorption percent for both CF-RH and CF-SCB is improved as the time increase until reaches the maximum sorption percent at time of 120 min (equilibrium time). The maximum sorption capacity of CF-RH and CF-SCB sorbents at equilibrium was 18.7 and 21.5 mg g^{-1} respectively. Prolong of reaction time higher than reaction equilibrium is characterized with slightly increase in sorption percent.

The kinetic of U(VI) sorption process using CF-RH and CF-SCB sorbents has been explored by analyzing the attained results using several kinetic models, namely, Lagergren and pseudo-second-order equations. The linear forms and the main concept of the kinetic models are displayed in Table S1 [9, 10]. The kinetic parameters are explored by plotting the relation between log (qe-qt) as a function of time (Fig. 9) and qt/t VIS time (Fig. 10) and presented in Table 1.

The acquired data in Table 1 declare that the sorption process is fitting well to the pseudo-second-order kinetic model for both applied sorbents since it possesses the highest coordination coefficient ($R^2 = 0.99$) and the calculated values of sorption capacity for CF-RH and CF-SCB (19.9 and 22.8 mg g^{-1} respectively) match with the experimental values (CF-RH: 18.7 mg g^{-1}; CF-SCB: 21.5 mg g^{-1}). This reflects that the rate-controlling step is chemisorption, and the sorption process achieved through a chemical reaction or electron sharing between the metal ions and the active function groups on the applied carbon fiber [42, 43]. The same kinetic profile has been reported for uranium(VI) sorption from aqueous solution using active carbon/PAN composite [14], activated carbon from wood wastes [15], and *phosphorylated luffa rattan activated carbon* [16]. It is worth noted that the sorption capacity of SCB is higher than that of RH sorbent which could be owned to that SCB sorbent possess higher number of function groups than the other one. Therefore, the chemical interaction during the adsorption process is favorable since both adsorbents have limited surface characteristics, particularly, limited pore volumes which exhibit higher tendency to chemical binding with uranium species. The comparison between the kinetic profile of CF-RH and CF-SCB declares that the half equilibrium time the initial sorption rate for both sorbents; CF-RH ($t_{1/2}$: 36.3 h; h: 0.55 mol g^{-1} h^{-1}) and CF-SCB ($t_{1/2}$: 33.5 h; h: 0.68 mol g^{-1} h^{-1}) are relatively close which indicates that U(VI) sorption process with both sorbents has almost the same equilibrium time.

from aqueous solution using active carbon/PAN composite [14], activated carbon from wood wastes [15], and *phosphorylated luffa rattan activated carbon* [16].

Fig. 8 Impact of shaken time on U(VI) sorption efficiency, % (2.0 g sorbent/ L; initial concentration 50 mg L.$^{-1}$; temperature 298 K; pH 4.01)
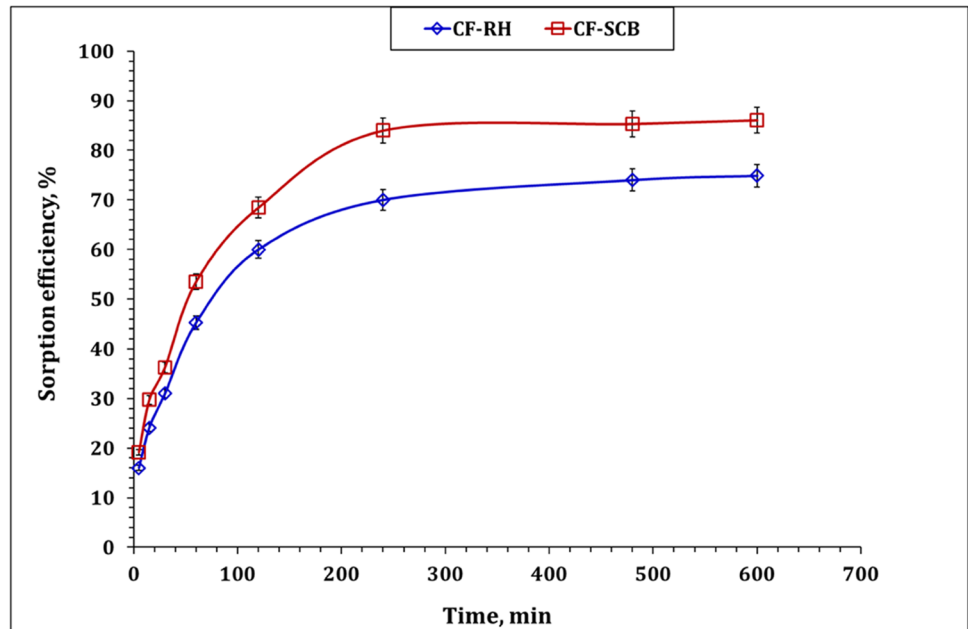
Fig. 9 Lagergren plot for uranium sorption onto CF-RH and CF-SCB sorbents
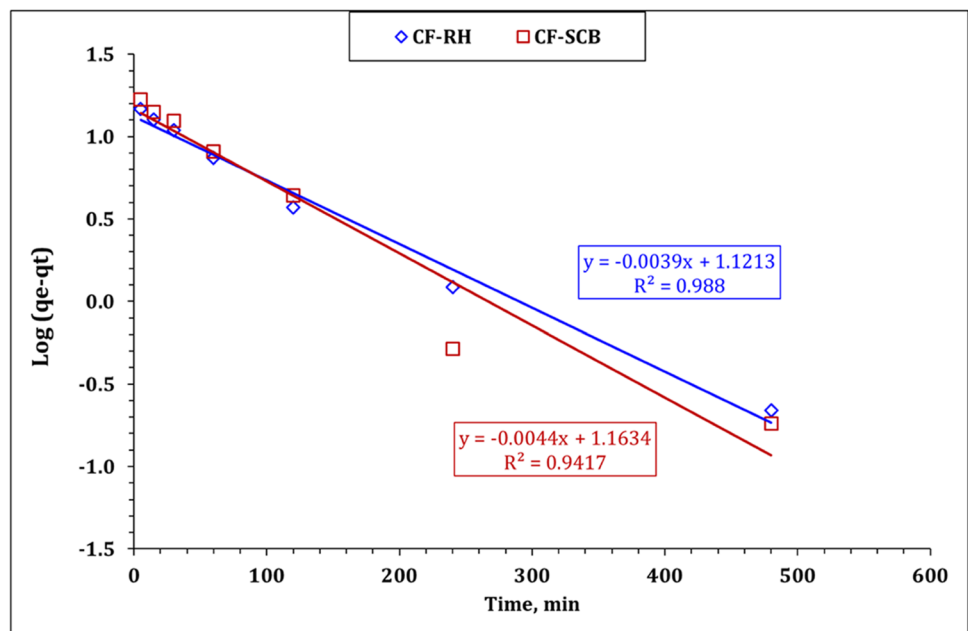
The sorption mechanism could be explored by analyzing the obtained data using Morris-Weber model. In accordance to this model, the U(VI) sorption reaction is controlled with solo mechanism in case the plot of qt as a function of time$^{0.5}$ (M-W plot) yield a linear relationship passing through the origin (one line segment); otherwise, the sorption reaction is controlled with multiple mechanisms if the plot yields numerous line segments [12, 13]. Weber and Morris model parameters are evaluated and presented in Table 1. Based on M-W plot (Fig. 11), it could be conducting that U(VI) sorption using RH and SCB sorbents is controlled with multiple mechanisms, whereas the plot consists of two line segments. The first-line segment which represents the first sorption stage depicted high rate of reaction which attributed to the fleet physical adsorption behavior. This behavior reflects that physical adsorption dominates the adsorbed behavior, while chemical adsorption

Fig. 10 Pseudo-second-order plot for uranium sorption onto CF-RH and CF-SCB sorbents
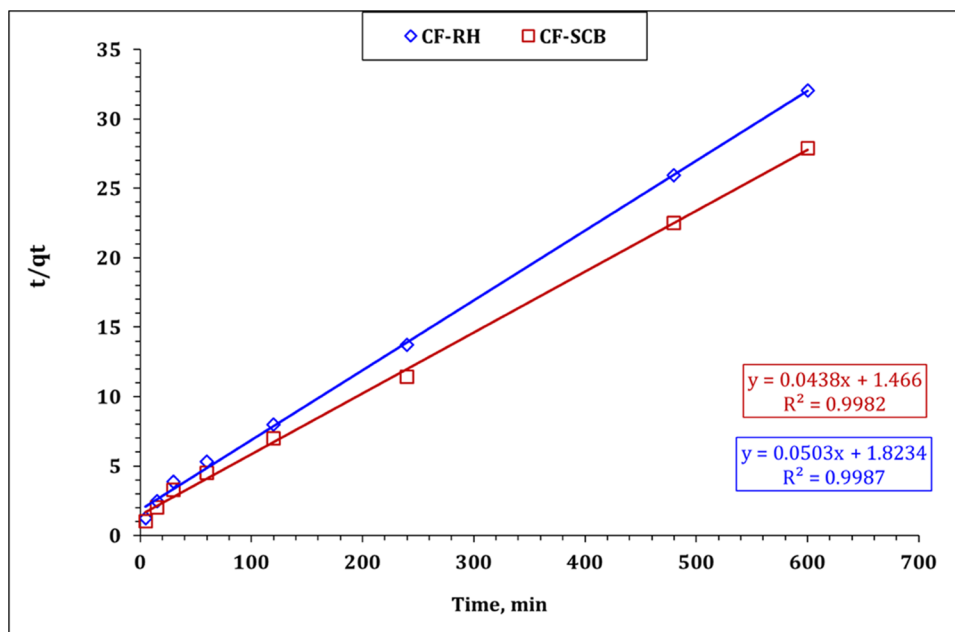
Table 1 The calculated parameters of the pseudo-first-order, pseudo-second-order, and Weber and Morris kinetic models

		CF-RH	CF-SCB
Lagergren pseudo-first-order	k_1 (min^{-1})	0.009	0.010
	qe$_{cal}$ (mg/g)	13.2	14.6
	qe$_{exp}$ (mg/g)	18.7	21.5
	R^2	0.68	0.68
Pseudo-second-order	k_2 (min^{-1})	0.001	0.001
	qe$_{cal}$ (mg/g)	19.9	22.8
	qe$_{exp}$ (mg/g)	18.7	21.5
	h (mol g^{-1} h^{-1})	0.55	0.68
	$t_{1/2}$ (h)	36.3	33.5
	R^2	0.99	0.99
Weber and Morris model	Stage I		
	k_i (mg/g min$^{1/2}$)	1.06	1.24
	C	2.2	2.6
	R^2	0.97	0.98
	Stage II		
	k_i (mg/g min$^{1/2}$)	0.14	0.06
	C	15.4	20.1
	R^2	0.98	0.99

is responsible for a very small portion [44]. The second stage (represented by the line segment) obvious slow rate of reaction which could be owned to the saturation of sorbent surface active sites; hence, the intraparticle diffusion mechanism (pore or surface diffusion) takes place under the impact of gradient U(VI) concentration [42–44].

3.2.3 Effect of temperature and reaction thermodynamics

The impact of reaction temperature range (25–60 °C) on uranium (VI) sorption from aqueous solution using RH and SCB sorbents has been performed at sorbent dose of 2 g L^{-1}, U(VI) initial concentration of 50 mg L^{-1}, for 240 min. The acquired data (Fig. 12) depicted that the sorption percent enhanced for both materials as the reaction temperature increase which reflects the endothermic nature of the U(VI) sorption process. The thermodynamic parameters (i.e., Gibbs free energy change (ΔG), entropy change (ΔS) and enthalpy change (ΔH)) could be attained from the thermodynamic equation displayed in Table S1 and tabulated in Table 2 [45, 46]. The variation of log kc with 1/T (Fig. S1) was applied to evaluate the standard enthalpy change (ΔH^o). The explored results confirming that the U(VI) process is endothermic, whereas the ΔH^o has positive values for RH and SCB sorbents (CF-RH: 33.1, and CF-SCB: 22.0) [10]. The negative values of ΔG^o for all investigated temperature range exhibit the spontaneous and feasibility of U(VI) sorption using RH and SCB materials [30, 31]. The positive value of ΔS^o (CF-RH: 171.1, and CF-SCB: 140.5) obvious the increase of randomness at the sorbent surface due to the sorption process [13]. Aslani and Amik [14], Zhang et al. [16], and Alahabadi et al. [15] mentioned that uranium ions sorption from aqueous solution using active carbon/PAN composite, *phosphorylated luffa rattan activated carbon*, and activated carbon from wood wastes, respectively, is an endothermic, spontaneous, and feasible sorption process which is consistent with the obtained data in this work.

Fig. 11 Morris-Weber illustration for uranium adsorption onto CF-RH and CF-SCB sorbents
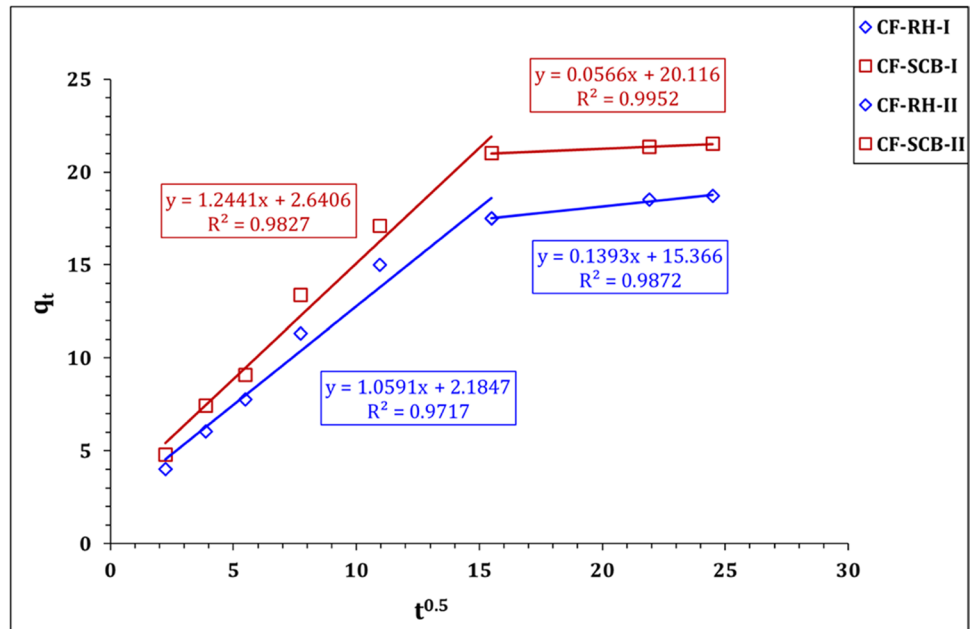
Fig. 12 Effect of sorption temperature on uranium removal percent, % (U(VI) initial concentration 50 mg L.$^{-1}$; shaking time 240 min; sorbent dose 2 g/L; pH 4.01)
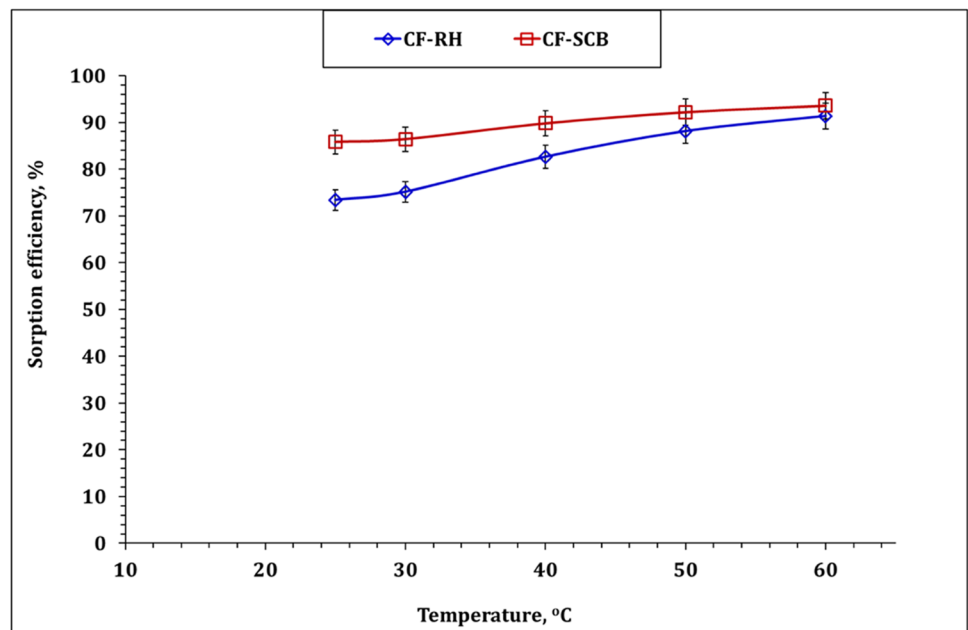
Table 2 Thermodynamic parameters for uranium sorption onto CF-RH and CF-SCB sorbents

	ΔG (kJ/ mol)				ΔH	ΔS
	20 °C	30 °C	40 °C	50 °C	(kJ/ mol)	(J/ mol K)
CF-RH	− 17.9	− 18.4	− 20.2	− 22.1	33.1	171.1
CF-SCB	− 19.9	− 20.3	− 21.8	− 23.3	22.0	140.5

3.2.4 Equilibrium studies of isotherm adsorption

Uranium sorption ability versus U(VI) initial concentration can display optimal adsorption efficiency of the prepared sorbents. In this regard, a set of experiments was carried out using sorbent dose of 2 g/L, pH of 4.03, room temperature (298 ± 1 K), and mixing time of 240 min, while U(VI) initial concentration was varied from 20 to 300 mg L^{-1}.

The anticipated results in Fig. 13 explore that CF-RH and CF-SCB sorbents exhibit the same sorption performance, whereas as the initial concentration increases, the sorption efficiency % decreases while the sorption capacity increases.

The isotherm performance of U(VI) sorption onto CF-RH and CF-SCB sorbents could be anticipated by fitting the acquired results using Langmuir and Freundlich isotherm models. The linear form of the applied models is presented in Table S1 [45, 46]. The variation of C_e/q_e as a function of C_e (Fig. 14) is used to obtain the Langmuir isotherm parameters, while the Freundlich isotherm variables were evaluated from the relation between log q_e and log C_e (Fig. 15). The acquired isotherm parameters are shown in Table 3. The attain data obvious that Langmuir plot (Fig. 14) exhibits perfect linear relationship ($R^2 = 0.99$) for both sorbents which reflect that the experimental results are fitting well to this model. This means that the sorption can be described as a monolayer cover for CF-RH and CF-SCB sorbents, and both sorbents possess a homogeneous distribution of the surface-active sites [42, 43]. Besides, the sorption capacity follows the following rank: CF-SCB ($29.1 \ mg \ g^{-1}$) > CF-RH ($21.0 \ mg \ g^{-1}$) which is consistent

Fig. 13 Effect of U(VI) initial concentration on uranium removal percent, % (room temperature; shaking time 240 min; sorbent dose 2 g/ L; pH 4.03)
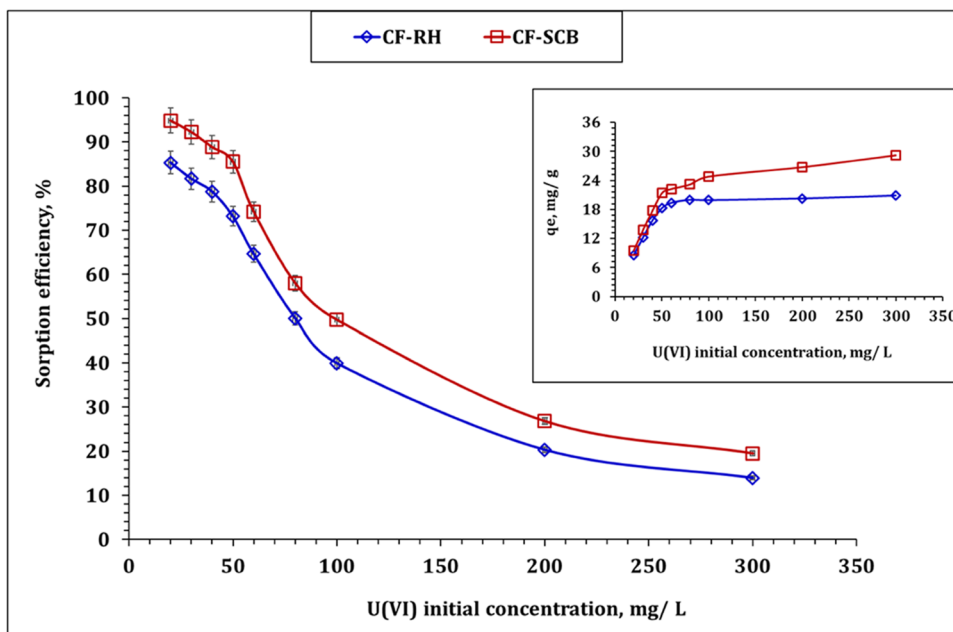
Fig. 14 Langmuir isotherm graph for U(VI) sorption onto CF-RH and CF-SCB sorbents
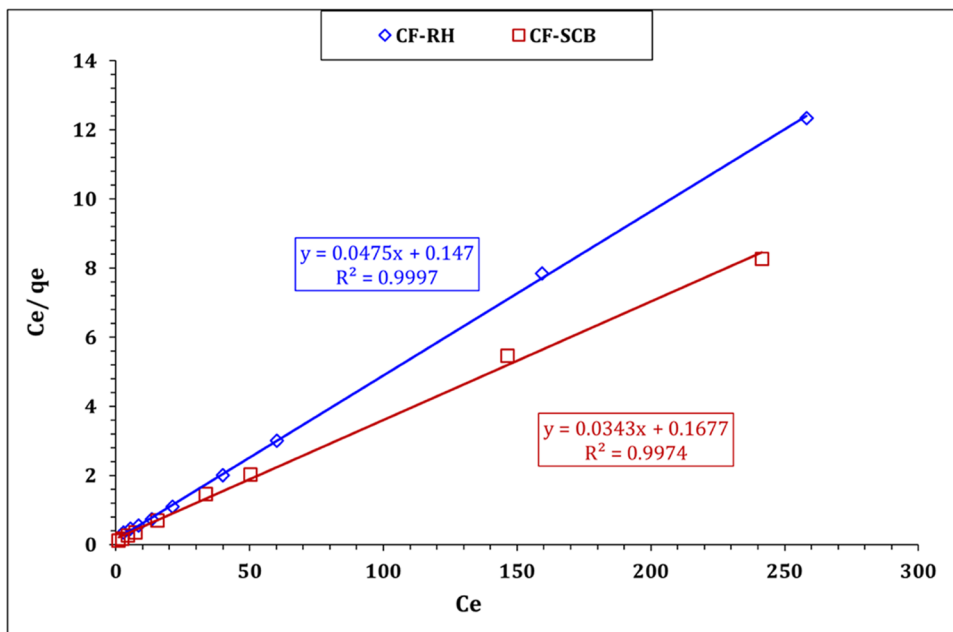
Fig. 15 Freundlich isotherm graph for U(VI) sorption onto CF-RH and CF-SCB sorbents
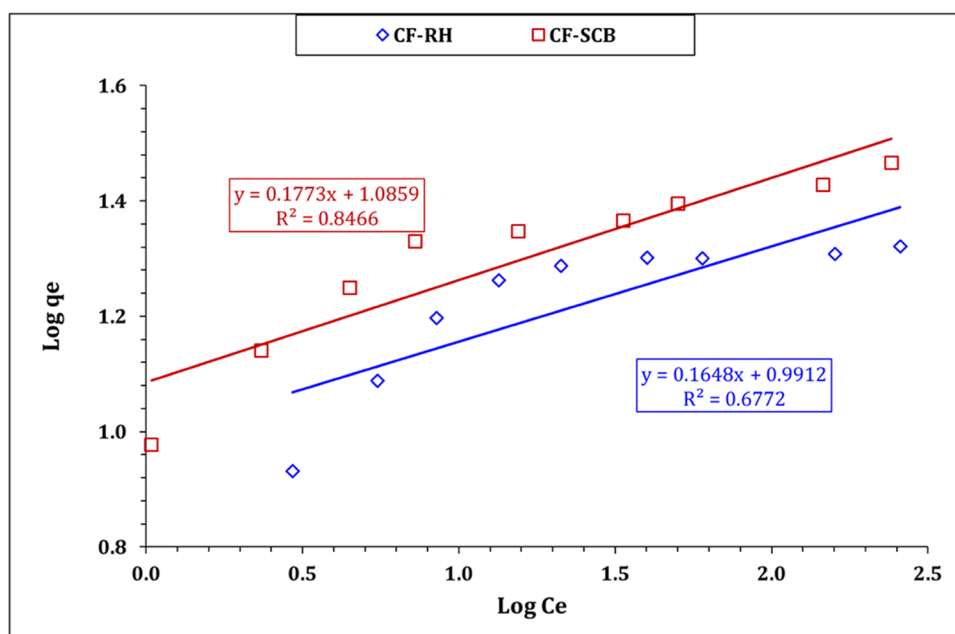
Table 3 Freundlich and Langmuir isotherm parameters for U(VI) sorption onto CF-RH and CF-SCB sorbents

		CF-RH	CF-SCB
Freundlich isotherm model	K_f (mg/g)	9.80	12.19
	n	6.07	5.64
	R^2	0.67	0.84
Langmuir isotherm model	Q_m (mg/g)	21.05	29.15
	b (L/mg)	0.323	0.970
	R^2	0.99	0.99

with the kinetic findings. The same sorption profile has been reported by Aslani and Amik [14], Zhang et al. [16], and Alahabadi et al. [15] for uranium ion sorption from aqueous solution using active carbon/PAN composite, *phosphorylated luffa rattan* activated carbon, and activated carbon from wood wastes, respectively.

The sorption capacity of the applied sorbents is displayed in Table 4 in comparison with the sorption capacity of other carbonaceous sorbents from literatures. The obtained data declare that both CF-RH and CF-SCB sorbents are considered as potential materials for cleaning contaminated aqueous solution from uranium species.

3.2.5 Impact of sorbent dose

The variation of sorption percent as a function of sorbent (i.e., CF-RH and CF-SCB) amount of addition (0.5–4 g L^{-1}) has been investigated at the following parameters: U(VI) initial concentration of 50 mg L^{-1}, mixing time of 240 min, and room temperature. The dependency of sorption percent on sorbent dose is displayed in Fig. 16. As expected, the sorption percent improved as the sorbent dose increases. This performance is owned to the occurrence of more high-activity particles and more active

Table 4 Comparison of sorption performance of U(VI) for different carbon sorbents

C_o, mg L^{-1}	Temp, °C	pH	Time, h	Q_e, mg g^{-1}		Ref
25–125	30	3.0	3.0	8.6	*Pistacia vera* L. shell-activated carbon	[47]
20–240	30	6.0	2.5	16.3	Hazelnut shell-activated carbon	[48]
10–80	25	10.0	7	53.2	Modified rice husk biochar	[49]
5–100	20	4.0	6	19.4	Fungus *Pleurotus ostreatus*	[50]
20–300	25	5.5	1	27.2	Eucalyptus wood biochar	[51]
2–60	45	4.0	24	52.6	Rice husk magnetic biochar composites	[52]
10–400	30	4.0	2	28.2	active carbon/polyacrylonitrile composite	[14]
20–300	**25**	**4.0**	**4**	**21.05**	**CF-RH**	**PW**
20–300	**25**	**4.0**	**4**	**29.15**	**CF-SCB**	**PW**

*PW, present work

Fig. 16 Impact of sorbent amount of addition on uranium sorption efficiency, % (U(VI) initial concentration 50 mg L.$^{-1}$; shaking time 240 min; temperature 298 K; pH 4.01)
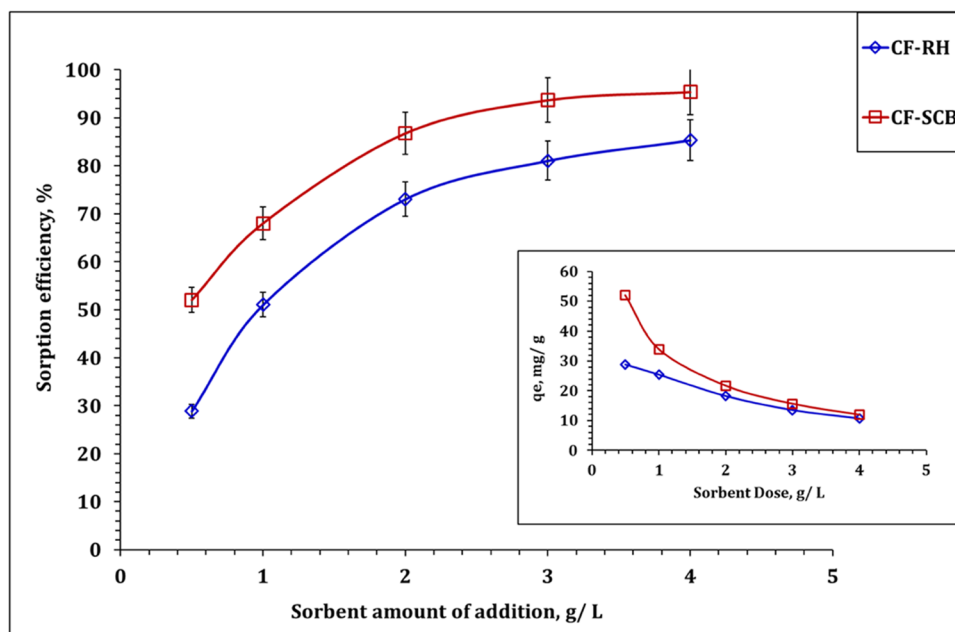
sites [9, 10]. Sorbent dose ≥ 3 g/L displayed a slightly increase in the sorption percent. Within the same sorbent dose range, the sorption capacity is depicted by a ramp down which could be attributed to clothing of the material, and a lower increase in vacancy places could take place, because of the increase of the sorbent amount. Moreover, the low concentration of U(VI) ions is not equivalent to the sorbent adsorption capacity and thereby decreased the qe [12, 13]. Sorbent dose of 3 g/L was selected for other experiments.

3.2.6 Uranium elution and adsorbent reusability

Designing a new sorbent and a sorption process also requires optimizing the metal desorption for valorizing the metal, concentrating the hazardous contaminant and for recycling the sorbent. In accordance, U(VI) elution from the loaded CF-SCB sorbent (which gives the heist sorption capacity) was performed using 1.0 M of different solutions, namely, sulfuric, nitric, and hydrochloric acids. The experimental conditions were: 3.0 g L^{-1} sorbent dose, room temperature, and shaking time 12 h. The acquired data in Table S2 obvious that sulfuric acid solution exhibit the highest elution efficiency (91.2%). The stability of the prepared CF-SCB carbonaceous material for recycling has been investigated by introducing the sorbent for five sorption/desorption sequence cycles. The attained results in Table S3 declare that the sorption and desorption percent slightly changed from 92.0 to 89.6% for sorption process and from 91.4 to 88.4% for desorption process over the five cycles, which reflects the feasibility of sorbent recycling.

3.2.7 Liquid raffinate treatment

Uranium removal from liquid effluent is an important process for environmental security. In accordance, the prepared CF-SCB sorbent has been applied for U(VI) sorption from wastewater produced at the Nuclear Materials Authority. The main components of the raffinate solution were Ca(II) and Fe(III) concentrations of 0.64 and 0.33 g L^{-1}, nitric acid molarity of 0.5 M, and U(VI) concentration of 50 mg L^{-1} as measured using ICP-AES. The application experiment was performed according to the following parameters: solution pH of 3.01, shaking time of 240 min, room temperature, and sorbent dose of 3 g L^{-1}. Subsequent filtration was conducted, and U(VI) concentration was measured using ICP-AES. The attained results display that CF-SCB materials successfully removed about 90.2% of U(VI) from the raffinate solution, which reflects that the applied carbon sorbent is a good alternative material for the liquid waste remediation process.

4 Conclusion

Successful utilization of agricultural waste-based carbon fiber for wastewater treatment process is introduced as an interesting approach, in this study, for both environmental and water security perspectives. In particular, efficient thermal treatments of rice husk and sugar cane bagasse could produce two respective carbon fiber materials, namely, CF-RH and CF-SCB. The structural, textural, and surface charge characteristics of the prepared fibrous materials were confirmed using XRD, FTIR, Raman, BET surface area, zeta, and TEM analyses. The prepared structures

could reveal efficient capture for uranium species from contaminated aqueous solution using batch adsorption method. Increased sorption capacity of 21.0 and 29.0 mg g^{-1} could be respectively attained by CF-RH and CF-SCB. Kinetic investigation displayed that U(VI) sorption process, by both carbon fibers, is achieving equilibrium level within 240 min and is of chemisorption nature. Isotherm study could conclude that the sorbets behavior is strongly matched with Langmuir model. Additionally, thermodynamic analysis clarified the endothermic fit of the adsorption process while being spontaneous and feasible. In conclusion, it can be clearly stated that the presented carbon fibers, as sorbets, could be of successful potential as valuable environmentally friendly engineering materials for the disposal of uranium in effluent aqueous solution.

Supplementary information The online version contains supplementary material available at https://doi.org/10.1007/s13399-022-03097-6.

Author Contribution *Ayman F. Abou-Hadid*: Conceptualization, Supervision, and Reviewing. *Usama A. El-Behairy*: Conceptualization, Supervision, and Reviewing. *Mahmoud M. Elmalih*: Experimental operation, Data interpretation, and Writing–editing. *Enas Amdeha*: Synthesis, Characterization, Data curation and interpretation, and Writing–original draft. *Ahmed M. A. El Naggar*: Methodology, Investigation, Data curation and interpretation, and Writing–original draft, reviewing, and editing. *Mohamed H. Taha*: Methodology, Validation, Data curation and interpretation, and Writing–original draft, reviewing, and editing. *Ahmed E. M. Hussein*: Conceptualization, Supervision, and Reviewing.

Declarations

Conflict of Interests The authors declare no competing interests.

References

1. Karić N, Maia AS, Teodorović A, Atanasova N, Langergraber G, Crini G, Ribeiro ARL, Đolić M (2022) Bio-waste valorisation: agricultural wastes as biosorbents for removal of (in)organic pollutants in wastewater treatment. Chem Eng J Adv 9:100239. https://doi.org/10.1016/J.CEJA.2021.100239

2. Khan FA, Tomar A, Agarwal YK, Shukla HO (2021) Agricultural Solid Waste Management: An Approach to Protect the Environment and Increase Agricultural Productivity. Handb Solid Waste Manag pp. 1–27. https://doi.org/10.1007/978-981-15-7525-9_28-1

3. Boechat CL, Arauco AM de S, Duda RM, et al (2017) Solid Waste in Agricultural Soils: An Approach Based on Environmental Principles, Human Health, and Food Security. Solid Waste Manag Rural Areas. https://doi.org/10.5772/intechopen.69701

4. Akash S, Sivaprakash B, Raja VCV, Rajamohan N, Muthusamy G (2022) Remediation techniques for uranium removal from polluted environment – review on methods, mechanism and toxicology. Environ Pollut 302:119068. https://doi.org/10.1016/J.ENVPOL.2022.119068

5. Ye Y, Al-Khaledi N, Barker L, Darwish MS, El Naggar AM, El-Yahyaoui A Haneklaus N (2019) Uranium resources in China's phosphate rocks–identifying low-hanging fruits. IOP Conf Ser Earth Environ Sci 227: 052033. IOP Publishing. https://doi.org/10.1088/1755-1315/227/5/052033

6. Melo D, Burkart W (2019) Uranium: Environmental pollution and health effects. Encycl Environ Heal pp. 252–258. https://doi.org/10.1016/B978-0-444-63951-6.00658-6

7. Appukuttan D, Rao AS, Apte SK (2006) Engineering of Deinococcus radiodurans R1 for bioprecipitation of uranium from dilute nuclear waste. Appl Environ Microbiol 72:7873–7878. https://doi.org/10.1128/AEM.01362-06/ASSET/1B6548FD-06AC-4D40-A81E-F41E07874A1E/ASSETS/GRAPHIC/ZAM0120673280006.JPEG

8. Gu B, Liang L, Dickey MJ, Yin X, Dai S (1998) Reductive precipitation of uranium(VI) by zero-valent iron. Environ Sci Technol 32:3366–3373. https://doi.org/10.1021/ES980010O

9. Ye T, Liu Z, Cai Z (2020) Adsorption of uranium(VI) from aqueous solution by novel dibutyl imide chelating resin. J Radioanal Nucl Chem 323:223–232. https://doi.org/10.1007/s10967-019-06949-0

10. Masoud AM (2020) Sorption behavior of uranium from sulfate media using purolite A400 as a strong base anion exchange resin. Int J Environ Anal Chem pp. 1–23. https://doi.org/10.1080/03067319.2020.1763974

11. Yang F, Xie S, Wang G, Yu CW, Liu H, Liu Y (2020) Investigation of a modified metal-organic framework UiO-66 with nanoscale zero-valent iron for removal of uranium (VI) from aqueous solution. Environ Sci Pollut Res 27:20246–20258. https://doi.org/10.1007/S11356-020-08381-4/FIGURES/16

12. Kanjilal A, Singh KK, Tyagi AK et al (2021) Synthesis of bi-functional chelating sorbent for recovery of uranium from aqueous solution: sorption, kinetics and reusability studies. J Polym Res 28:460. https://doi.org/10.1007/s10965-021-02819-0

13. Wang CL, Li Y, Liu CL (2015) Sorption of uranium from aqueous solutions with graphene oxide. J Radioanal Nucl Chem 304:1017–1025. https://doi.org/10.1007/s10967-014-3855-x

14. Aslani CK, Amik O (2021) Active Carbon/PAN composite adsorbent for uranium removal: modeling adsorption isotherm data, thermodynamic and kinetic studies. Appl Radiat Isot 168:109474. https://doi.org/10.1016/J.APRADISO.2020.109474

15. Alahabadi A, Singh P, Raizada P, Anastopoulos I, Sivamani S, Dotto GL, Landarani M, Ivanets A, Kyzas GZ, Hosseini-Bandegharaei A (2020) Activated carbon from wood wastes for the removal of uranium and thorium ions through modification with mineral acid. Colloids Surf A Physicochem Eng Asp 607:125516. https://doi.org/10.1016/J.COLSURFA.2020.125516

16. Zhang Y, Ye T, Wang Y, Zhou L, Liu Z (2021) Adsorption of uranium(VI) from aqueous solution by phosphorylated luffa rattan

activated carbon. J Radioanal Nucl Chem 327:1267–1275. https://doi.org/10.1007/S10967-020-07592-W

17. El Naggar AMA, Ali MM, Abdel Maksoud SA, Taha MH, Morshedy AS, Elzoghby AA (2019) Waste generated bio-char supported co-nanoparticles of nickel and cobalt oxides for efficient adsorption of uranium and organic pollutants from industrial phosphoric acid, J Radioanal Nucl Chem 320 741–755

18. Cuña A, Ortega Vega MR, da Silva EL, Tancredi N, Radtke C, Malfatti CF (2016) Nitric acid functionalization of carbon monoliths for supercapacitors: effect on the electrochemical properties, Int J Hydrogen Energy 41 12127–12135. https://doi.org/10.1016/j.ijhydene.2016.04.169

19. Sheldon RA (2016) Green chemistry, catalysis and valorization of waste biomass. J Mol Catal A Chem 422:3–12. https://doi.org/10.1016/j.molcata.2016.01.013

20. Li Q, Ma CL, Zhang PQ, Li YY, Zhu X, He YC (2021) Effective conversion of sugarcane bagasse to furfural by coconut shell activated carbon-based solid acid for enhancing whole-cell biosynthesis of furfurylamine. Ind Crops Prod 160:113169

21. Gautam N, Kate G, Chaurasia A (2020) Upgrading of rice husk char obtained by pyrolysis process to amorphous silica and activated carbon. Mater Today Proc 39:1382–1385. https://doi.org/10.1016/j.matpr.2020.04.859

22. Ali MM, Abedelmaksoud SA, Taha MH, El Naggar AMA, Morshedy AS, Elzoghbi AA (2020) Uranium separation from phosphoric acid using metallic carbonaceous structures as efficient adsorbents: an experimental and kinetic study. Radiochemistry 62(2):204–215

23. Badawy NA, El-Bayaa AA, Amdeha E (2015) Removal of Cu (II), Ni (II), and Co (II) ions from aqueous solution using low cost adsorbent: isotherms, kinetics and equilibrium aspects. J Chem Pharm Res 7:589–598

24. Amdeha E (2021) Recovery of nanomaterials from agricultural and industrial wastes for water treatment applications, in: A.S.H. Makhlouf, G.A.M. Ali (Eds.), Waste Recycl Technol Nanomater Manuf Springer Cham. pp 385–417. https://doi.org/10.1007/978-3-030-68031-2_14

25. Siddiqui MF, Khan SA, Hussain D, Tabrez U, Ahamad I, Fatma T, Khan TA (2022) A sugarcane bagasse carbon-based composite material to decolor and reduce bacterial loads in waste water from textile industry. Ind Crops Prod 176:114301. https://doi.org/10.1016/j.indcrop.2021.114301

26. Jarernboon W, Iamtipueng P, Pimanpang S (2018) Preparation of the natural carbon fiber from narrow-leaved cattails (Typha angustifolia Linn .) flower for using as the cathode catalyst in the zinc-air fuel cell. Mater Today Proc 5 14002–14008

27. Chaudhuri B, Ghosh S, Mondal B, Bhadra D (2022) Preparation and characterization of carbon fibre powder (CFP)-polyvinyl alcohol (PVA) composite films showing percolation threshold behaviour, Mater Sci Eng B Solid-State Mater Adv Technol 275 115500. https://doi.org/10.1016/j.mseb.2021.115500

28. Liu F, Wang H, Xue L, Fan L, Zhu Z (2008) Effect of microstructure on the mechanical properties of PAN-based carbon fibers during high-temperature graphitization. J Mater Sci 43:4316–4322. https://doi.org/10.1007/s10853-008-2633-y

29. Poursorkhabi V, Abdelwahab MA, Misra M, Khalil H, Gharabaghi B, Mohanty AK (2020) Processing, carbonization, and characterization of lignin based electrospun carbon fibers: a review. Front Energy Res 8:208. https://doi.org/10.3389/fenrg.2020.00208

30. Taha MH, Abdel Maksoud SA, Ali MM, El Naggar AMA, Morshedy AS, Elzoghby AA (2019) Conversion of biomass residual to acid-modified bio-chars for efficient adsorption of organic pollutants from industrial phosphoric acid: an experimental, kinetic and thermodynamic study, Int J Environ Anal Chem 99 1211–1234. https://doi.org/10.1080/03067319.2019.1618459

31. Inyang MI, Gao B, Yao Y, Xue Y, Zimmerman A, Mosa A, Pullammanappallil P, Ok YS, Cao X (2016) A review of biochar as a low-cost adsorbent for aqueous heavy metal removal. Crit Rev Environ Sci Technol 46(4):406–433. https://doi.org/10.1080/10643389.2015.1096880

32. Yeasmin MS, Mondal MIH (2015) Synthesis of highly substituted carboxymethyl cellulose depending on cellulose particle size. Int J Biol Macromol 80:725–731. https://doi.org/10.1016/j.ijbiomac.2015.07.040

33. Roy D, Kanojia S, Mukhopadhyay K, Eswara Prasad E (2021) Analysis of carbon-based nanomaterials using Raman spectroscopy: principles and case studies. Bull Mater Sci 44 1–9. https://doi.org/10.1007/s12034-020-02327-9

34. Chailuecha C, Klinbumrung A, Chaopanich P, Sirirak R (2021) Graphene-like porous carbon nanostructure from corn husk: synthesis and characterization. Mater Today Proc 47:3525–3528. https://doi.org/10.1016/j.matpr.2021.03.512

35. Kołodziej A, Długoń E, Świętek M, Ziąbka M, Dawiec E, Gubernat M, Michalec M, Wesełucha-Birczyńska A (2021) A raman spectroscopic analysis of polymer membranes with graphene oxide and reduced graphene oxide. J Compos Sci 5:20. https://doi.org/10.3390/jcs5010020

36. Ruiz-Rosas R, Bedia J, Lallave M, Loscertales IG, Barrero A, Rodríguez-Mirasol J, Cordero T (2010) The production of submicron diameter carbon fibers by the electrospinning of lignin. Carbon N Y 48:696–705. https://doi.org/10.1016/j.carbon.2009.10.014

37. Alothman ZA (2012) A review: fundamental aspects of silicate mesoporous materials. Materials (Basel) 5:2874–2902. https://doi.org/10.3390/ma5122874

38. Habibi MK, Rafiaei SM, Alhaji A, Zare M (2022) Synthesis of ZnFe2O4: 1 wt% Ce3+/carbon fibers composite and investigation of its adsorption characteristic to remove Congo red dye from aqueous solutions. J Alloys Compd 890:161901. https://doi.org/10.1016/j.jallcom.2021.161901

39. Taer E, Iwantono, Yulita M, Taslim R, Subagio A, Salomo, Deraman M (2013) Composite electrodes of activated carbon derived from cassava peel and carbon nanotubes for supercapacitor applications, AIP Conf Proc 1554 70–74. https://doi.org/10.1063/1.4820286

40. E. Taer, D. Afdal Yusra, A. Amri, Awitdrus, R. Taslim, Apriwandi, Agustino, A. Putri (2020) The synthesis of activated carbon made from banana stem fibers as the supercapacitor electrodes. Mater Today Proc 44 3346–3349. https://doi.org/10.1016/j.matpr.2020.11.645

41. Usha Rani M, Nanaji K, Rao TN, Deshpande AS (2020) Corn husk derived activated carbon with enhanced electrochemical performance for high-voltage supercapacitors. J Power Sources. 471 228387. https://doi.org/10.1016/j.jpowsour.2020.228387

42. Kong L, Ruan Y, Zheng Q, et al (2020) Uranium extraction using hydroxyapatite recovered from phosphorus containing wastewater. J Hazard Mater 382:120784. https://doi.org/10.1016/j.jhazmat.2019.120784

43. Huang Y, Zheng H, Li H, et al (2020) Highly selective uranium adsorption on 2-phosphonobutane-1,2,4-tricarboxylic acid-decorated chitosan-coated magnetic silica nanoparticles. Chem Eng J 388:124349. https://doi.org/10.1016/j.cej.2020.124349

44. Wu W, Chen D, Li J et al (2018) Enhanced adsorption of uranium by modified red muds: adsorption behavior study. Environ Sci Pollut Res 25:18096–18108. https://doi.org/10.1007/s11356-018-2027-x

45. B.S. Marques, Frantz TS, Sant'Anna Cadaval Junior TR, de Almeida Pinto LA, Dotto GL (2019) Adsorption of a textile dye onto piaçava fibers: kinetic, equilibrium, thermodynamics, and application in simulated effluents, Environ Sci Pollut Res Int 26 28584–28592. https://doi.org/10.1007/S11356-018-3587-5

46. Kang HJ, Kim JH (2019) Adsorption kinetics, mechanism, isotherm, and thermodynamic analysis of paclitaxel from extracts of Taxus chinensis cell cultures onto sylopute, biotechnol. Bioprocess Eng 2019 243. 24 513–521. https://doi.org/10.1007/S12257-019-0001-1

47. Donat R, Erden KE (2017) Adsorption of U(VI) ions from aqueous solutions by activated carbon prepared from Antep pistachio (Pistacia vera L.) shells. Radiochim Acta 105 359–367. https://doi.org/10.1515/RACT-2016-2637/MACHINEREADABLE CITATION/RIS

48. Zhu M, Liu R, Chai H, Yao J, Chen Y, Yi Z (2016) Hazelnut shell activated carbon: a potential adsorbent material for the decontamination of uranium(VI) from aqueous solutions. J Radioanal Nucl Chem 310:1147–1154. https://doi.org/10.1007/S10967-016-5011-2/FIGURES/6

49. Bin Zhang Z, Cao XH, Liang P, Liu YH (2013) Adsorption of uranium from aqueous solution using biochar produced by hydrothermal carbonization. J RadioanalNucl Chem 295 1201–1208. https://doi.org/10.1007/S10967-012-2017-2/FIGURES/12

50. Zhao C, Liu J, Tu H, Li F, Li X, Yang J, Liao J, Yang Y, Liu N, Sun Q (2016) Characteristics of uranium biosorption from aqueous solutions on fungus Pleurotus ostreatus. Environ Sci Pollut Res Int 23:24846–24856. https://doi.org/10.1007/S11356-016-7722-X

51. Mishra V, Sureshkumar MK, Gupta N, Kaushik CP (2017) Study on Sorption Characteristics of Uranium onto Biochar Derived from Eucalyptus Wood. Water Air Soil Pollut 228:1–14. https://doi.org/10.1007/s11270-017-3480-8

52. Li M, Liu H, Chen T, Dong C, Sun Y (2019) Synthesis of magnetic biochar composites for enhanced uranium(VI) adsorption. Sci Total Environ 651:1020–1028. https://doi.org/10.1016/J.SCITOTENV.2018.09.259